On the near surface momentum balance in the Yucatán Channel

M. Marín[1]*, J. Candela[1], J. Sheinbaum[1], J. Ochoa[1] and A. Badan[1]

[1]Departamento de Oceanografía Física, Centro de Investigación Científica y Educación Superior de Ensenada, Ensenada, Baja California, México

Resumen

Se analizó el balance horizontal de momento en la capa superior de Canal de Yucatán para un periodo de 22 meses de septiembre de 1999 a junio de 2001, usando datos de corrientes superficiales de mediciones de ADCPs de ocho anclajes localizados a través del canal, datos de presión de mediciones de sensores de presión a ambos lados del canal, vientos de QUICKSCAT y datos de altimetría de AVISO. El balance promedio entre Isla Mujeres, México, y Cabo San Antonio, Cuba, (a través del canal) es básicamente geostrófico con contribuciones de los términos ageostroficos, en particular de la fricción contra la capa inferior y en menor grado el flujo de Ekman en la superficie. Los términos advectivos así como el término de la aceleración local parecen no tener importancia en el balance promediado de lado a lado del canal. Es interesante notar que a lo largo del canal el balance promedio es principalmente geostrófico mientras que la fricción lineal, el flujo de Ekman, así como los términos de aceleración local y advectivos permanecen sin importancia. Realizando un análisis del balance de anclaje a anclaje a través del canal se encontró que en la zona donde la corriente de Yucatán oscila, los términos advectivos con derivadas en la dirección a través del canal si contribuyen significativamente al balance dinámico. Se obtuvieron FEOs de las anomalías del nivel del mar de altimetría y de los primeros 90 metros del flujo a lo largo del canal encontrando que existe relación entre ellos donde los primero modos (altimetría y flujo) parecen estar relacionados con la variabilidad del transporte a través del canal y también están asociados con el gradiente de presión a lo largo del canal y la oscilación del núcleo de la corriente, sugiriendo que existe una considerable interacción de remolinos con la corriente en el Canal.

Palabras clave: Canal de Yucatán, balance de momento, dinámica de canal, geostrofía.

Abstract

The horizontal momentum balance in the upper layers of the Yucatán Channel is examined for a period of 22 months, from September 1999 to June 2001, using subsurface currents from ADCP measurements at eight moorings across the channel, pressure measurements from coastal pressure sensors on both sides of the channel, QuickSCAT winds and AVISO altimetry data. The averaged balance between Isla Mujeres, México, and Cabo San Antonio, Cuba, (across-channel axis) is basically geostrophic, but with contributions from ageostrophic terms, particularly friction against lower layers and to a lesser degree, the surface Ekman drift. Both the advective and the local acceleration terms appear unimportant in the side-to-side averaged balance. Interestingly, the averaged balance in along-channel axis is also mainly geostrophic; linear friction, Ekman drift, local acceleration and advective terms remain unimportant. An analysis of the balance from mooring to mooring across the channel indicates that in the region where the Yucatán current meanders, the advective terms with across-channel derivatives contribute significantly. The EOF modes of sea level anomalies from altimetry and the along-channel flow in the upper 90 m surface layer are correlated. Their two first modes are seemingly related to the transport fluctuations through the channel, but also to the along-channel pressure gradient and to the meandering of the Yucatán Current core, suggesting the presence of appreciable eddy-current interactions in the Channel.

Key words: Yucatán Channel, momentum balance, channel dynamics, geostrophy.

Introduction

The Yucatán channel, a region of strong currents and high variability, is located between the Yucatán peninsula and the western tip of the island of Cuba; it connects the Caribbean Sea with the Gulf of Mexico across an approximate width of 200 km and a maximum sill depth of 2040 m. The flux through the channel is that part of the North Atlantic Subtropical Gyre flow that enters the Caribbean through several passages between the lesser and greater Antilles, and continues onward across the Caribbean Sea to

comes the Loop Current, and proceeds towards the Florida Straits to feed the Gulf Stream (Murphy and Hurlburt, 1999; Schmitz and McCartney, 1993).

The intense current in the western part of the Yucatán Channel that flows toward the Gulf of Mexico with speeds of 120 cm/s at the surface down to 10 cm/s at 800 m depth is the Yucatán Current. The along-channel subinertial flow fluctuations across the Yucatán Channel are larger than their mean except within the Yucatán Current (Abascal et al., 2003). Close to Cuba, an intermittent flow

with a mean of about 10 cm/s toward the Caribbean Sea is known as the Cuban Countercurrent. There, in the deeper part is a midchannel vertical band of flow (<10 cm/s), into the Gulf of Mexico with countercurrents on both sides, which constitute a three banded structure distribution of weaker mean currents (Ochoa et al., 2001; Sheinbaum et al., 2002). The low frequency variations in the deep flows have been found to be related to the Loop Current extension (Bunge et al., 2002). The average total transport that passes through the channel, measured over the 22 month-long period between September 1999 to June 2001, is 22.8±1 Sv (1 Sv = $10^6 m^3 s^{-1}$) with a standard deviation (due to subinertial motions) of 3.3 Sv (Ochoa et al., 2003; Abascal et al., 2003). This mean is smaller than the expected 28 Sv based on previews historical hydrographic surveys and flow measurements (Sheinbaum et al., 2002). The nature of the fluctuations is important, since shedding of mesoescale anticyclonic rings requires notably a growth and extended Loop Current into the Gulf of Mexico and but also a triggering mechanism such as the passage of a cyclone, burst of a positive vorticity flux or other intermittent dynamic process (Candela et al., 2002; Zavala-Hidalgo et al., 2006). Some numerical simulations (Candela et al., 2003) support this conjecture, but others not (Oey, 2004). No detailed study of the momentum balance governing the Yucatán Channel surface flow has been made, although Emilsson (1971) suggest from limited observations that the currents are predominantly inertial.

The momentum balance equates the local acceleration, advective and Coriolis terms to the pressure gradient term, external forcing and dissipative terms. Here the rule in these kind of calculations are the parameterizations in dynamical models, in order to describe the contributions of different terms in the horizontal momentum balance, since measurements are never complete. These analyses help infer currents from measurements of other oceanographic variables (Bryden, 1977; Viudez et al., 1999). Studies carried out in the straits of Gibraltar (Candela et al., 1989) and that of Eripus (Tsimplis, 1997) found that the transverse balance is principally geostrophic, i.e. with the pressure gradient balancing the Coriolis term. Though, in the straits of Dover (Prandle and Player 1993) and Belle Isle (Garrett and Toulany. 1981), the wind also plays an important role in the balance. In dynamical terms, the Yucatán Channel is neither a channel or a strait because it is neither sufficiently long or narrow in terms of its first internal Rossby radius of deformation of 44 km (computed with respect to the sill depth of 2040 m) (Ochoa. et al., 2001). This precludes the a priori assumption that the balance in the Yucatán Channel has a dynamic behavior similar to that found in these previous studies. Here the initial dynamical model is more general and is then tested for consistency against the observations.

Studies of Western Boundary currents, as they cross through straits or channels, have shown that wind and eddies can be important factors in modifying the volume transport. For the Florida Straits, Anderson and Corry (1985), Lee, Schott and Zantopp (1985), Lee and Williams (1988) among others, found that variations of the wind stress curl both upstream (Caribbean) and downstream (Gulf Stream) as well as along-channel winds could contribute to the annual volume transport cycle of the Florida current, whereas for the Kuroshio Current, volume transport variations within the East Taiwan Channel are linked to a meandering pattern associated with the arrival of mesoscale eddies from the western Pacific on time-scales of order 100-days (Zhang et al., 2001; Johns et al., 2001). In these two regions, a strong relationship exists between volume transport and sea level difference across the strait or channel. (Maul et al., 1990; Johns et al., 2001). It is then natural to ask if such relationship might hold in the Yucatán Channel, and if not, whether the wind and intermittent eddies might be important to the kinematics and dynamics of this system.

After a description of the data used for the term evaluation in section 2, we define in sections 3 and 4 the terms in the horizontal momentum equations and describe how each term is approximated. Then in section 5 the average momentum balance is analyzed, first between Isla Mujeres and Cabo San Antonio (across-channel axis) and later in the perpendicular direction (along-channel axis). The spectral relation between the most important terms is investigated in section 6. This is followed in section 7 by a more detailed study of the structure of the im portant across-channel terms and in section 8 by a statistical analysis of how the altimetry and current fields are related. Section 9 presents a discussion and brief summary of the main results.

Data

The data include current measurements obtained from 8 moorings across the Yucatán Channel (Fig. 1), with Aanderaa current meters and upward-looking ADCPs, for a period of 22 months from September 1999 to June 2001. The geographically oriented horizontal current components from these instruments were rotated counterclockwise by 19.59° to obtain across (u) and along-channel (v) current components aligned with the topography, with reference coordinates x, y and z for the across-, along-channel and vertical directions. This orientation is that of the line joining the pressure sensors on the two sides of the channel, and of the distribution of the mooring array across the channel (Fig. 1). These rotated currents coincide with the orientation of the principal axis of the surface current variability ellipses in the channel. Therefore, the variability along the new coordinate axis is maximized, and the momentum balance analysis becomes more efficient.
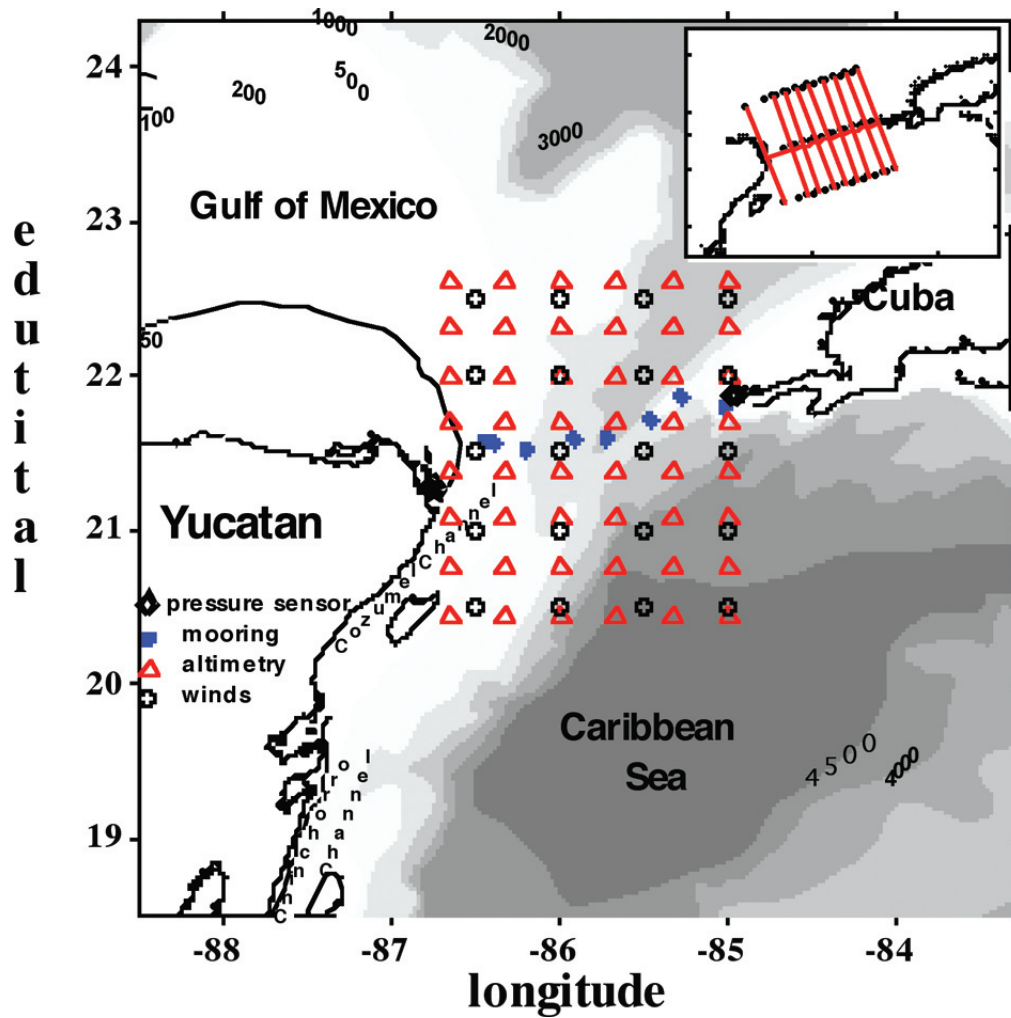
Fig. 1. Map of the Yucatan channel showing depth contours in m. and indicating the locations of the pressure sensors, moorings, altimetry and wind data grid. The inset shows the points where the data were interpolated

Subsurface pressure series for the same measurement period provided by two pressure sensors, one at Isla Mujeres, on the Yucatán side, 3 meters deep and the other at Cabo San Antonio, Cuba, at a depth of 10 meters (Fig. 1).

The altimetry data is available from the Archiving Validation and Interpretation of Satellite Oceanographic Data program (AVISO), providing maps of the sea level anomalies (SLA) on a mesh of 0.25° X 0.25° every 7 days throughout the study period. The altimetry information was interpolated to eleven specific transects in the channel; one between the pressure sensors and ten transects parallel to the channel cross section (Fig. 1), distributed across the channel, except for the one closest to the Yucatán Peninsula, and chosen to coincide with the pressure sensor at Isla Mujeres.

The SLA measurements over the two pressure sensors and the pressure measurements have correlation coefficients of 0.83 and 0.77 for Isla Mujeres and for Cabo San Antonio respectively, (Figs. 2a and 2b). The spectra of SLA and pressure in Figs. 2c and 2d show similar structures for both locations, although for the case of Cabo San Antonio the SLA has a larger energy content at lower frequencies, consistent with the result of Abascal et al. (2003), where low-frequency flow fluctuations predominate in the upper eastern side, denoting the frequent reversals of the Cuban Countercurrent. These high correlations support the use of the altimetry in this particular region despite the proximity to land. The pressure time series include a seasonal signal, with higher elevations in winter with respect to summer, and larger amplitudes and higher frequency content on the Yucatán side.

Wind stress was calculated from wind speed inferred by the QuickSCAT project with a mesh resolution of 0.5° X 0.5°. The wind stress was obtained using the Large and Pond (1981) expressions, and interpolated to the same transects used for the altimetry.
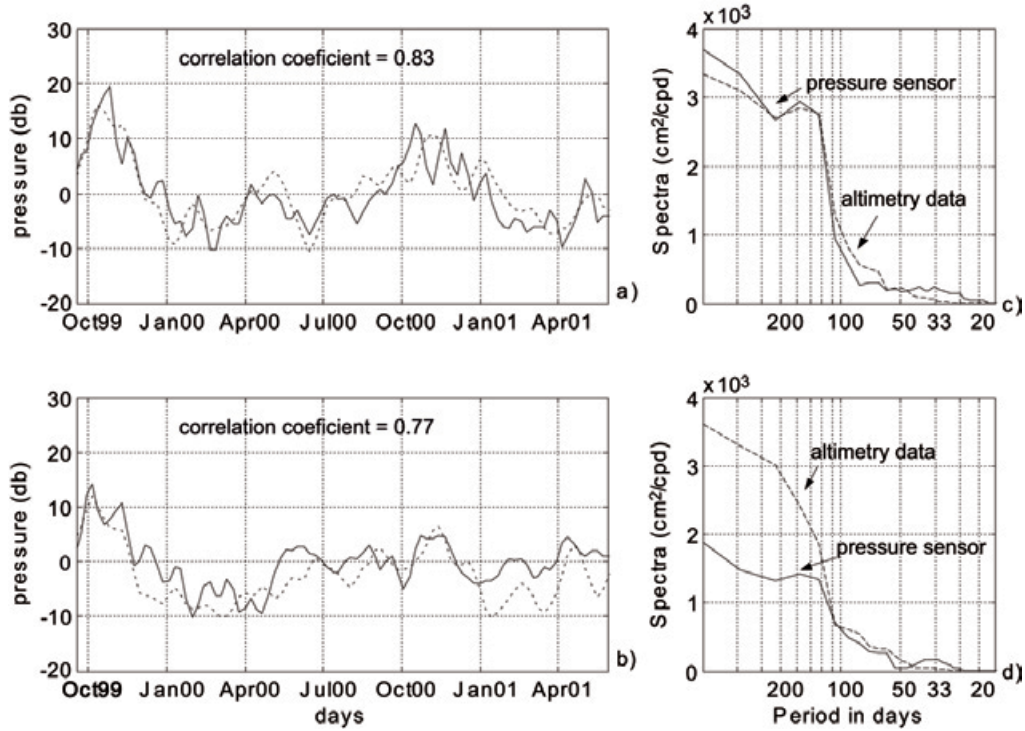
Fig. 2. Relation between pressure sensor measurements (solid line) and altimetry data (doted line) at a) Isla Mujeres and b) Cabo San Antonio. Power spectra of pressure (solid line) and altimetry data (doted line) for c) Isla Mujeres and d) Cabo San Antonio.

Horizontal momentum balance

Since we only have pressure or surface altimetry data to estimate the pressure gradients, the momentum balance in Yucatán Channel was analyzed only for the upper part of the water column assuming those pressures to be representative of depths of approximately 90 meters.

This study analyzes the momentum balance for fluctuations longer than 20 days (i.e, frequencies smaller than 1/20 cycles per day (cpd)). The velocity components in the across-, along-channel and vertical directions (u, v and w) and the pressure (P) are decomposed into low- and high-passed frequency parts via a Lanczos low-pass filter with a cutoff frequency of 1/20 cpd. The triangular brackets and the primes, in expressions like $u = <u>+ u´$, distinguish the low- and high-passed frequency contributions, thus <Q> denotes the filtering operation on Q.

Decomposing the variables in low-pass and fluctuating parts, assuming that $<<u>> = <\vec{u}>$ and $<u'> = 0$, and using the continuity equation (i.e. $\nabla \bullet u$), it follows that

$$\frac{\partial <u>}{\partial t}+\frac{\partial <uu>}{\partial x}+\frac{\partial <uv>}{\partial y}+\frac{\partial <uw>}{\partial z}+\frac{\partial <u'u'>}{\partial x}+$$
$$\frac{\partial <u'v'>}{\partial y}+\frac{\partial <u'w'>}{\partial z}-f<v>=-\frac{1}{\rho}\frac{\partial <P>}{\partial x} \quad , \quad (1)$$

$$\frac{\partial <v>}{\partial t}+\frac{\partial <uv>}{\partial x}+\frac{\partial <vv>}{\partial y}+\frac{\partial <vw>}{\partial z}+\frac{\partial <u'v'>}{\partial x}+$$
$$\frac{\partial <v'v'>}{\partial y}+\frac{\partial <v'w'>}{\partial z}+f<u>=-\frac{1}{\rho}\frac{\partial <P>}{\partial y} \quad . \quad (2)$$

(1) and (2) are the low-frequency horizontal momentum balance equations, where *t* is time, *f* the Coriolis parameter and ρ a reference density.

From these equations, an averaged momentum balance can be computed through horizontal and vertical integration across the channel. Since the vertical velocity is small and of the same order as the instrument error, the terms involving low-pass vertical velocities were dropped, but the turbulent stresses that include the fluctuating vertical velocity were retained. The vertical integration of these terms in (1) and (2) can be expressed in terms of vertical of horizontal momentum fluxes at the top and bottom of the layer being considered, i.e., the wind stress at the sea surface as boundary condition and the interfacial stress at the bottom of the layer modeled, was considered to the first order, as proportional to the across-channel velocity, as a Raleigh-type dissipation. That is,

$$-\frac{1}{h}\int_{z=-h}^{z=surface}\frac{\partial <w'u'>}{\partial z}dz\equiv\frac{1}{h}\frac{\tau_{x,WIND}-\tau_{x,z=-h}}{\rho}\oplus\frac{\tau_x}{\rho h}-\lambda u \quad (3)$$

$$-\frac{1}{h}\int\limits_{z=-h}^{z=surface}\frac{\partial <w'v'>}{\partial z}dz \equiv \frac{1}{h}\frac{\tau_{y,WIND}-\tau_{y,z=-h}}{\rho}\oplus\frac{\tau_y}{\rho h}-\lambda v \quad , \quad (4)$$

where τ_x and τ_y are the horizontal components of the wind stress, h is the vertical scale of surface stress influence and λ is a constant friction coefficient.

Thus, the momentum equations for the low-frequency motions are

$$\int\limits_{x=IslaM}^{x=CSanAz=surface}\int\limits_{z=-h}[\frac{\partial u}{\partial t}+\frac{\partial\, uu}{\partial x}+\frac{\partial\, uv}{\partial y}+\frac{\partial <u'u'>}{\partial x}+\frac{\partial <u'v'>}{\partial y}-$$
$$fv]dxdz=-\frac{1}{\rho}\frac{\Delta P}{\Delta x}+\frac{\tau_x}{\rho h}-\lambda u, \quad\quad (5)$$

$$\int\limits_{x=IslaM}^{x=CSanAz=surface}\int\limits_{z=-h}[\frac{\partial v}{\partial t}+\frac{\partial\, uv}{\partial x}+\frac{\partial\, vv}{\partial y}+\frac{\partial <u'v'>}{\partial x}+\frac{\partial <v'v'>}{\partial y}-$$
$$fu]dxdz=-\frac{1}{\rho}\frac{\Delta P}{\Delta y}+\frac{\tau_y}{\rho h}-\lambda v, \quad\quad (6)$$

after removing the notation of the filtering operator for the low-pass terms.

Evaluation of terms

The velocity components u and v used in the calculation of the different terms in the balance were obtained from the objectively interpolated measured currents averaged over the first 90 m of the surface layer. The same filtering operation was applied to the velocity field to separate its low-pass and fluctuating parts. Then a vertical and across- channel average was calculated to obtain mean currents for both components.

A cross-channel average of $\partial P/\partial x$ was obtained from the difference between the pressures measured at Isla Mujeres and Cabo San Antonio, divided by the distance between the pressure gauges. To evaluate the term $\partial P/\partial y$ in the along-channel balance, ten transects perpendicular to the one across the channel were drawn between Isla Mujeres and Cabo San Antonio at the locations where current information was available, and then altimetry data was interpolated to the end points of these transects. The interpolated SLAs were converted to pressure in order to calculate the along-channel surface pressure gradient at each transect and then an average over all transects was computed to obtain the channel-averaged $\partial P/\partial y$ term.

The local acceleration terms $\partial u/\partial t$ and $\partial v/\partial t$ were calculated by centered finite differences from the data series,

$$\frac{\partial u}{\partial t}(t)\cong\frac{u(t+\Delta t)-u(t-\Delta t)}{2\Delta t}, \quad\quad (7)$$

using Δt of 1 day. Similarly for the term $\partial v/\partial t$.

The terms $\partial uu/\partial x$, $\partial <u'u'>/\partial x$ and $\partial <u'v'>/\partial x$, were calculated by integrating across-channel, for example

$$\int\limits_{x=IslaM}^{x=CSanzA}[\frac{\partial uu}{\partial x}]dx\cong\frac{u_{C.San.A}^2-u_{Isla.M}^2}{\Delta x} \quad , \quad\quad (8)$$

where $u_{Isla.M}$ is the velocity close to Isla Mujeres, $u_{C.San.A}$ is the velocity across the channel near Cabo San Antonio, and Δx is the distance between these points.

No direct current information exists of estimates for along-channel derivatives. But supposing that an element of fluid that crosses the Yucatán channel preserves its velocity during a certain interval of time (Δt of 1 day), a Δy can be obtained for the time $t+\Delta t$ as the along-channel velocity multiplied by Δt. Thence, terms such as $\partial uv/\partial y$, $\partial <u'v'>/\partial y$ and $\partial vv/\partial y$, $\partial <v'v'>/\partial y$ may be estimated to first order. Notice that with this approximation the local acceleration term would cancel with the advective term, *i.e.*, $\partial u/\partial t + v\,\partial u/\partial y = 0$. As shown below, local acceleration terms are small, and within the above approximation for Δy, advective or Reynolds stress terms involving meridional derivatives turn out to be small compared to the other terms.

For the Ekman drift an integrated value of wind stress was obtained over the transect, both for the τ_x and τ_y components. To calculate the Ekman drift term as well as the friction terms, the independent parameters h and λ were fitted using a least squares technique in

$$-fv=-\frac{1}{\rho}\frac{\Delta P}{\Delta x}+\frac{\tau_x}{\rho h}-\lambda u \quad , \quad\quad (9)$$

where v, τ_x and u are actually side to side average values. For the across-channel balance the best fit for h was 26 meters. Considering that the h scale is on the order of tens of meters in most oceanic conditions, we used for the along channel balance term the same value obtained in the across-channel component, i.e., 26 meters.

The best-fit coefficients for the linear frictional coefficients λ_u and λ_v were 2.41×10^{-5} sec^{-1} and 4.98×10^{-6} sec^{-1} respectively, which correspond to e-folding decay time scales of ~12h and ~55h, respectively.

Averaged momentum balance

Across-channel momentum balance

We calculated and rearranged the terms of equation (5) keeping the along-channel velocity on the left side (so all terms are expressed in velocity units) and correlated each term with the velocity (Table I) obtaining a significant

correlation coefficient of 0.51 with the pressure gradient term (Fig. 3a). Fig. 4 shows the time series of the most important across-channel terms. Althoug the dynamic balance is mainly between the velocity through the channel and the across-channel pressure gradient, the frictional and Ekman drift terms play a significant role, as can be appreciated in Fig. 4 and Table I. The correlation coefficient between the frictional term and the along-channel velocity is 0.55. If we add the pressure gradient and friction terms and correlate it with the velocity we find an increase in the correlation coefficient to 0.70 (Fig. 3b). Now if we also add the Ekman drift term, which has a correlation coefficient of 0.26 with the velocity, the correlation increases to 0.75 (Fig. 3c). The local acceleration term $\partial u/\partial t$ and the advective terms have no significant contribution in the averaged balance. The term $\partial uu/\partial x$ (see Equations 5 and 8) has a relatively high

Table 1

Correlation coefficient between the along channel velocity *v* and the terms calculated in the across-channel balance

Terms	Correlation coefficient	Standard deviation
$\dfrac{1}{f\rho}\dfrac{\partial P}{\partial x}$	0.51 ± 0.14	0.057
$\dfrac{1}{f\rho}\dfrac{\tau_x}{h}$	0.26 ± 0.16	0.019
$\dfrac{1}{f}\lambda u$	0.55 ± 0.13	0.047
$\dfrac{1}{f}\dfrac{\partial u}{\partial t}$	0.04 ± 0.13	0.003
$\dfrac{1}{f}\dfrac{\partial\,uu}{\partial x}$	-0.39 ± 0.19	0.013
$\dfrac{1}{f}\dfrac{\partial\,uv}{\partial y}$	0.08 ± 011	0.003
$\dfrac{1}{f}\dfrac{\partial\,\overline{u'u'}}{\partial x}$	0.12 ± 0.17	0.003
$\dfrac{1}{f}\dfrac{\partial\,\overline{u'v'}}{\partial y}$	0.13 ± 0.11	0.0001

negative correlation coefficient with the velocity -0.39, but its magnitude is insignificant in the average balance.

Fig. 4 show that the Ekman drift term has higher variability in winter than in summer. This can also be observed in the pressure data and to a lesser extent in the pressure gradient and in the along-channel velocity. The larger Ekman drift variability events in winter (Fig. 4), coincide with high variability events in the velocity and pressure gradient time series, which means that the Ekman drift fluctuations are an important source of surface current variability. Separating the along-channel velocity, pressure gradient and Ekman drift time series in winter and summer periods and correlating them, we found that the correlation coefficient between the velocity and the pressure gradient increases to (0.65) in winter, as well as the correlation coefficient between velocity and Ekman drift to (0.56), whereas that between velocity and friction diminished (0.47). In summer, the correlation coefficient between velocity and pressure gradient diminishes (0.33) and that between velocity and Ekman drift remains almost the same (0.44), whereas that between velocity and friction increases (0.52).

This seasonal behavior of the Ekman drift contribution, specifically its high variability in winter, is probably due to the passage of frontal systems (gales known as "Northers" or "Nortes" through the Gulf of Mexico. Though these winds have principally a north-south component, it seems that also their east-west component is important in this region; however, these events have short durations and under a filtering process appear less energetic. The situation along the Yucatán Channel is some how similar to that found in the Florida Straits (Lee et al., 1988), where a high correlation between wind and transport was observed during winter, when strong wind events occur, and a lower correlation resulted during the summer, characterized by moderate winds. This suggests that a seasonal behavior contributes locally to the annual transport cycle.

The currents at Chinchorro and Cozumel channels, south of the Yucatán channel are in geostrophic balance most of the time, except for periods 1 to 2 weeks long when large ageostrophic deviations happen. These appear to be related to a gradient wind balance (Chávez et al., 2003; Ochoa et al., 2005; Cetina et al., 2005). Such behavior of alternating periods of clearly defined geostrophy and ageostrophy appear not to take place in the Yucatán Channel.

Along-channel momentum balance
The cross-channel velocity and the along-channel pressure gradient have a significant correlation of 0.82, indicative of a definite geostrophic balance (Fig. 5, table
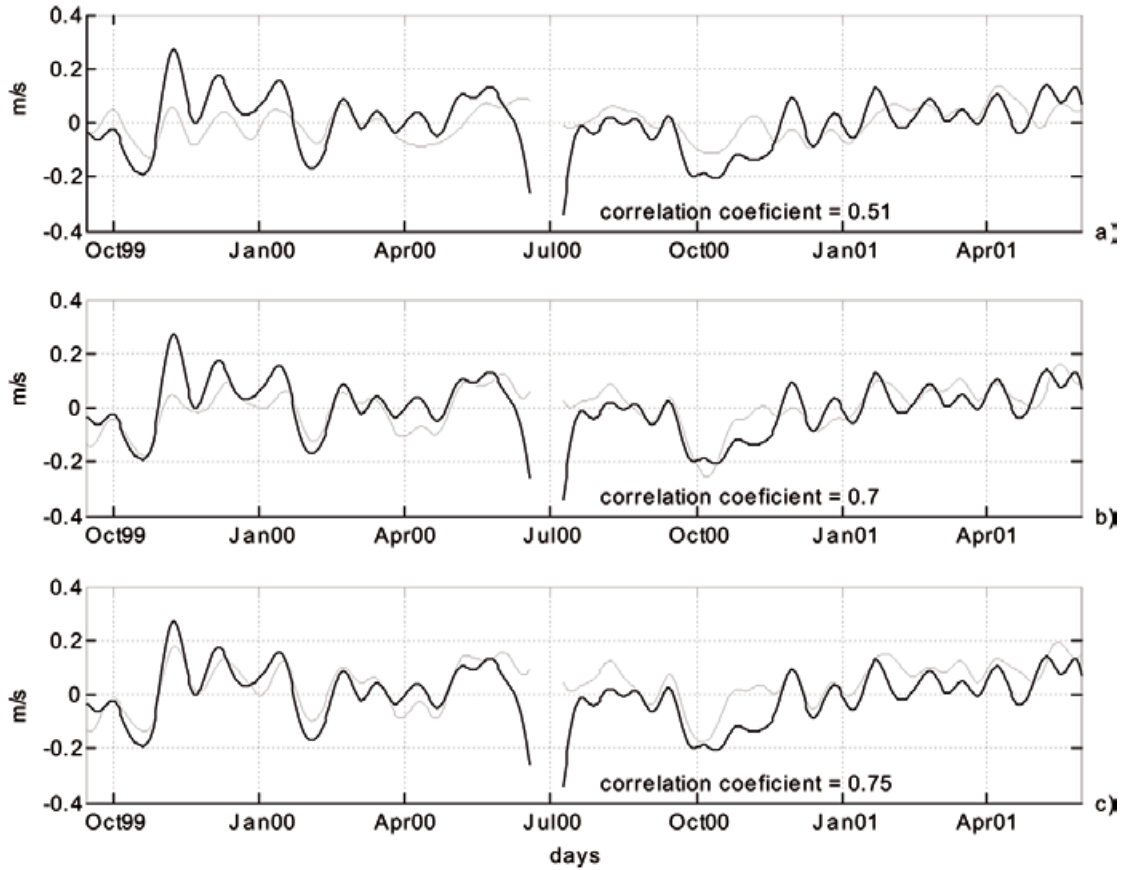
Fig. 3. Comparison between the different terms in the averaged across-channel momentum balance equation expressed in velocity units. a) Time series of along-channel current velocity (bold line) and across-channel pressure gradient (thin line). b) Time series of along-channel current velocity (bold line) and the across-channel pressure gradient plus linear friction term (thin line). c) Time series of along-channel current (bold line) and the sum of the pressure gradient, across-channel wind stress and frictional terms (thin line).

Fig. 4. Time series of the different terms calculated in the across-channel momentum balance in m/s. a) along-channel velocity. b) Pressure gradient term. c) Ekman drift term. d) Frictional term.

Fig. 5. Time series of across-channel current (bold line) and the along-channel pressure gradient (thin line).

Table 2

Correlation coefficient between the velocity u across channel and the terms calculated in the along-channel balance

Terms	Correlation coefficient	Standard deviation
$\dfrac{1}{f\rho}\dfrac{\partial P}{\partial y}$	0.82 ± 0.7	0.075
$\dfrac{1}{f\rho}\dfrac{\tau_y}{h}$	0.03 ± 0.19	0.025
$\dfrac{1}{f}\lambda v$	0.55 ± 0.13	0.009
$\dfrac{1}{f}\dfrac{\partial v}{\partial t}$	0.04 ± 0.11	0.003
$\dfrac{1}{f}\dfrac{\partial\, uv}{\partial x}$	-0.38 ± 0.19	0.030
$\dfrac{1}{f}\dfrac{\partial}{\partial y}vv$	0.06 ± 0.12	0.006
$\dfrac{1}{f}\dfrac{\partial\, \overline{u'v'}}{\partial x}$	-0.19 ± 0.18	0.003
$\dfrac{1}{f}\dfrac{\partial\, \overline{v'v'}}{\partial y}$	0.01 ± 0.10	0.0003

II), with the Ekman drift playing an insignificant role in the balance (correlation coefficient 0.02). Even if we add the pressure gradient and Ekman drift terms and correlate them with the cross-channel current, the correlation coefficient remains the same, and neither do the frictional, advective and local acceleration terms contribute to the along-channel balance. Fig. 6, shows the different terms in the along-channel balance.

A strong seasonal signal in the Ekman drift term is evident with high winter variability, similar to the one in the across-channel balance, also likely related to the "Nortes" or "Northers". On the contrary, a clear seasonal signal is missing both in the pressure gradient and the across-channel velocity terms. Separating the time series in winter and summer periods we note that the correlation coefficient between the across-channel current and along-channel pressure gradient is respectively 0.72 and 0.70, consistent with an important seasonal contribution to the correlation of 0.82 of the total series. The correlation coefficient between the velocity and the Ekman drift increases in winter (0.21) and is null in summer (0.00). The balance between the across-channel velocity and the along-channel pressure gradient terms seems to be related to the upper Yucatán Current transport variability, as is discussed below. Briefly stated, the mean along-channel momentum balance is essentially geostrophic, and this is an interesting and surprising result.

Spectral analysis

Spectral time series analysis of the different terms in the momentum equations were made using the Fourier transform with the Thomson multi-taper method (Percival and Walden, 1993). Spectra were calculated using 5 prolate spheroidal sequences "tapers" with 12 degrees of freedom.

Fig. 7 shows power spectra of the along-channel velocity and the across-channel pressure gradient. Both the velocity and the pressure gradient present two peaks at the 35 and 70 day periods, which have a significant coherence with a practically zero phase lag in the cross-spectra between these two series.

The spectra of the across-channel Ekman drift term (Fig. 8), shows peaks at periods of 80 and 33 days, and only the 33 day period band is significantly coherent with the along-channel velocity which lags the wind a couple of days at these periods. This could mean that the wind not only affects the velocity though the Ekman drift, which modifies the sea surface height, accumulating water
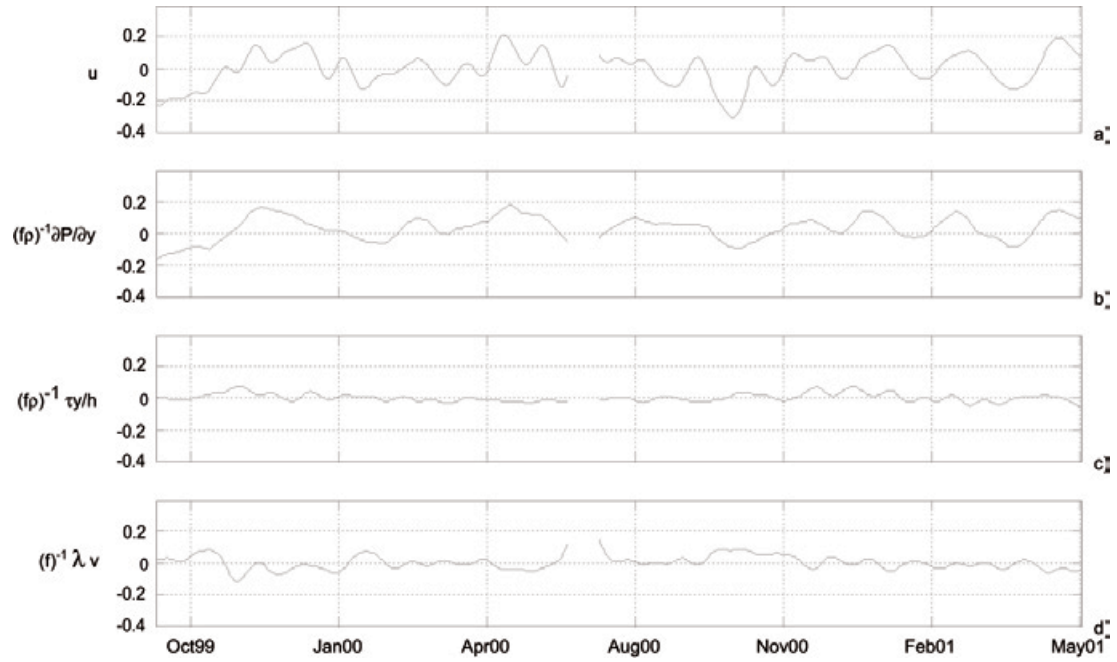
Fig. 6. Time series of the different terms calculated in the along-channel momentum balance in m/s. a) Across-channel velocity. b) Pressure gradient term. c) Ekman drift term. d) Frictional term.
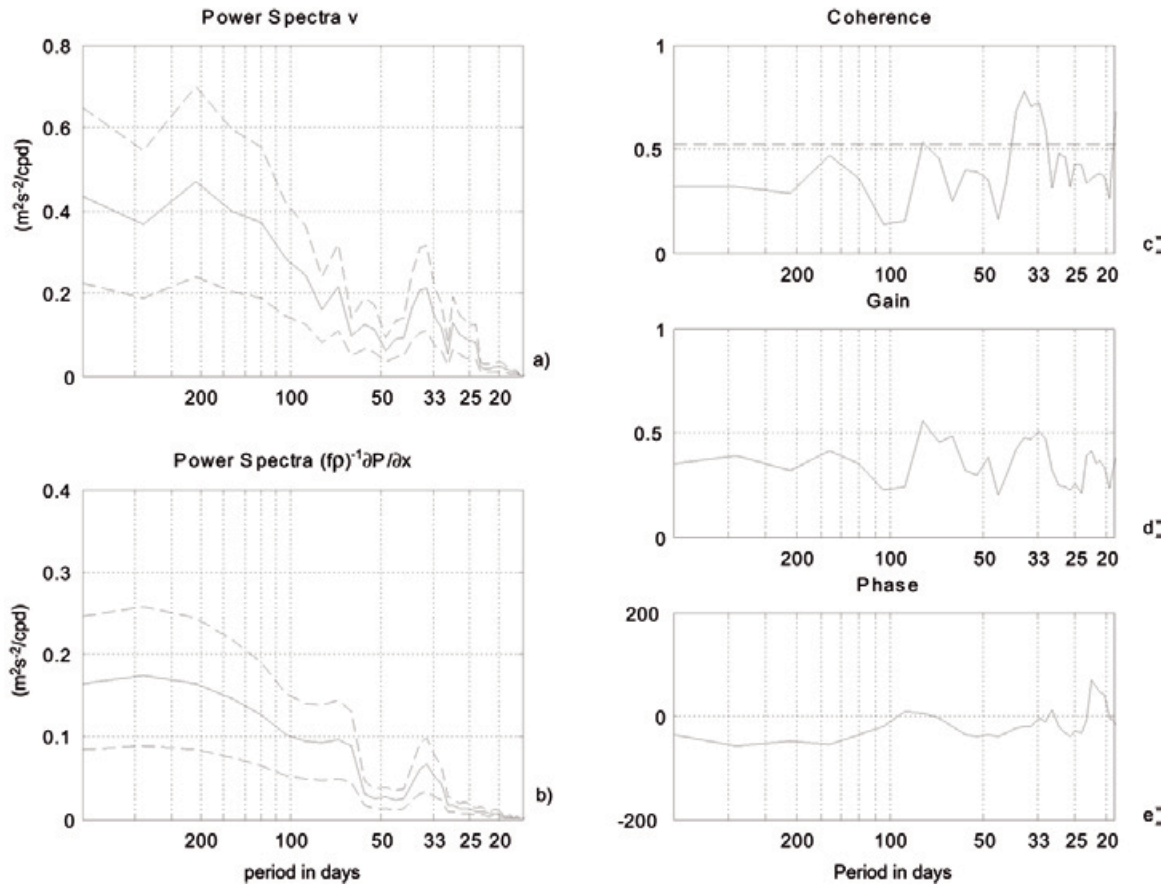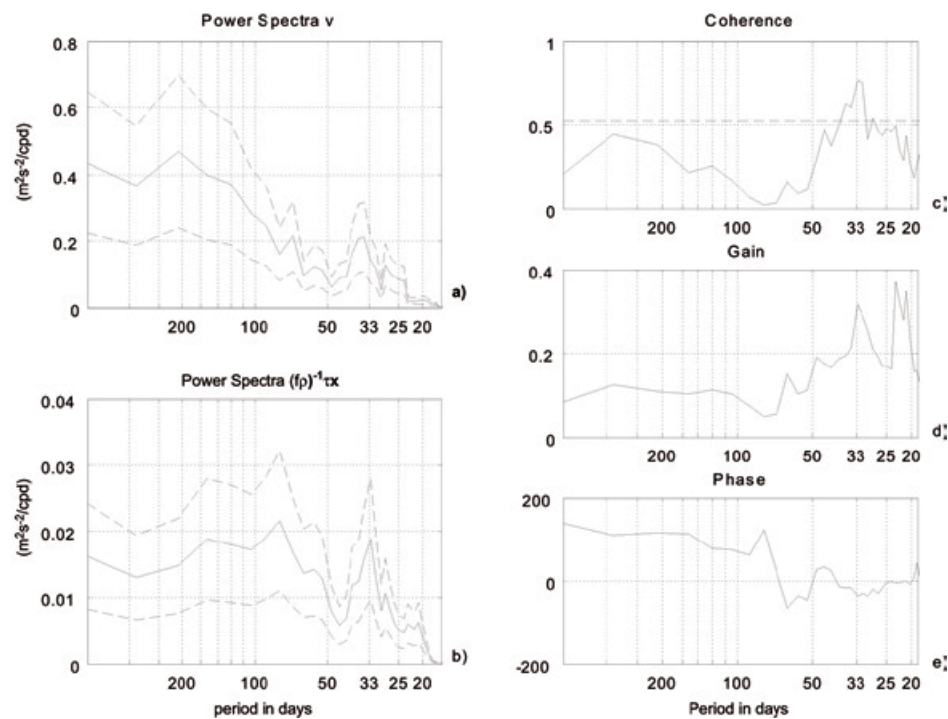

Fig. 7. Power spectra of along-channel velocity (a), across-channel pressure gradient (b) (in m²s⁻²/cpd). Coherence (c) Gain (d) and Phase (e), for the cross-spectra calculations between along-channel velocity and across-channel pressure gradient terms. Line in the coherence plot indicates the 95% confidence level.

Fig. 8. Power spectra of along-channel velocity (a), across-channel wind stress (b) (in m^2s^{-2}/cpd). Coherence (c) Gain (d) and Phase (in degrees) (e), for the cross-spectra calculations between along-channel velocity and across-channel wind stress terms. The horizontal line in the coherence plot indicates the 95% confidence level.
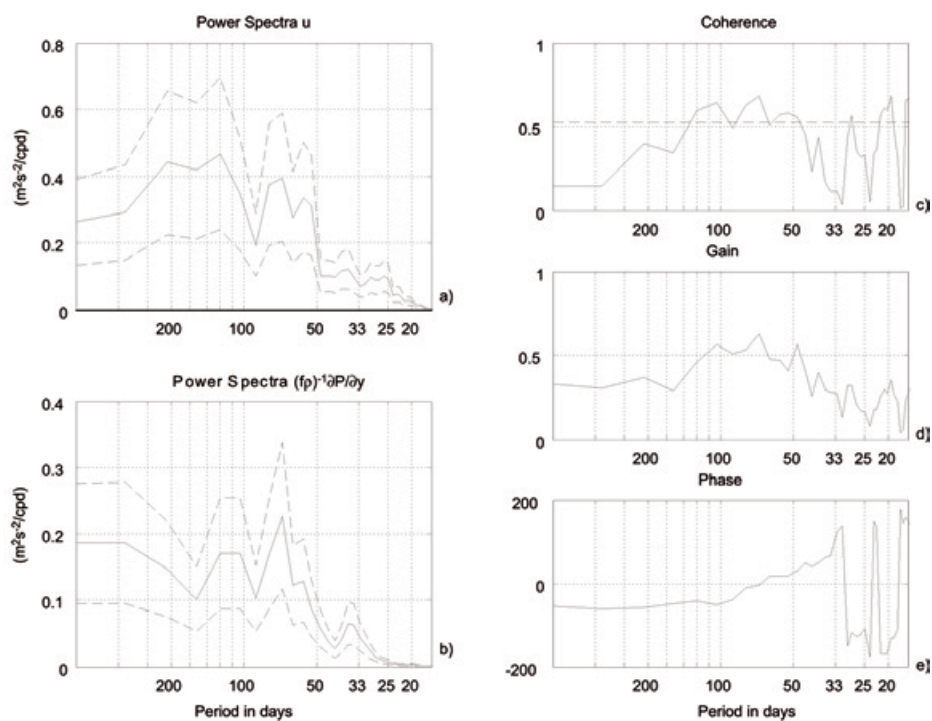
Fig. 9. Power spectra of across-channel velocity (a), along-channel pressure gradient (b). Coherence (c) Gain (d) and Phase (e), for the cross-spectra calculations between across-channel velocity and along-channel pressure gradient terms. The horizontal line in the coherence plot indicates the 95% confidence level.

on the sides of the channel and directly influencing the pressure gradient across the channel. This process comes to an equilibrium in a couple of days.

The cross-spectra between the along-channel velocity and the frictional term (not shown) presents coherent peaks at 70, 125 and 200 day periods with almost zero phase. These long periods could be associated with the 50-100 day-long events found by Guerrero (2005) in the region, attributed to the interaction of the Yucatán Current with the passage of eddies, a condition similar to what is observed at the Kusroshio Current when it flows through the East Taiwan Channel (Zhang et al., 2001).

The along-channel terms, the across-channel velocity and the along-channel pressure gradient power spectra exhibit well defined peaks at periods of 60, 70 and 125 days (Fig. 9). As mentioned previously, these periods could be associated with the passage of eddies thorough the channel, which explain the changes of the along-channel pressure gradient.

Structure of the momentum balance

Across-channel momentum balance

A more detailed analysis of the momentum balance was performed by evaluating the different terms in equation (5) at 15 points across the channel (Fig. 10a), using the surface velocity points of the objective mapping mesh and interpolating the SLA data to obtain the pressure gradients at these locations. Fig. 10b shows a time-series map of the along-channel velocity at the 15 points used for the analysis. High variability is present on both sides of the channel, especially on the Yucatán side, where the core of the Yucatán Current is located, while the variability at the center of the channel is much lower. The structure of the pressure gradient in Fig. 10d is similar to that of the velocity, but with a smaller magnitude. The correlation between velocity and pressure gradient time series is lower along the Yucatán side and increases towards the center of the channel (Fig. 10c). The lowest correlation is found within the zone of lateral meandering of the Yucatán Current core, (the core moves between longitude -86°40' and -86°18') suggestive of curvature in the flow that might be responsible for a loss of geostrophy in that area.

For the frictional term (which is proportional to the across-channel velocity component) the highest variability is observed at the center of the channel, coincident with the highest correlation with the along-channel current, whilst near the Yucatán Current the correlation is practically null, except for a western section close to the Yucatán coast (Figs. 11a and 11b). The Ekman drift term (not shown) is fairly constant across the channel,

and presents a smaller correlation with the along-channel current on the Yucatán side. Interestingly, the "$\partial uu/\partial x$" term (Fig. 11d) which apparently had no influence in the average momentum balance, presents magnitudes comparable to those of the pressure gradient and frictional terms on the west side of the channel where high variability is found, with maximum values during the winter periods and a correlation of -0.7 with the along-channel velocity (Fig. 11c). This suggests that in the western part of the channel this advective term significantly contributes to the balance, especially when the Yucatán Current is weak (compare Figs. 10b and 11d).

Along-channel momentum balance

The balance of terms in the along-channel direction is also analyzed at the same locations across the channel (Fig. 10a). The across-channel velocity shows higher variability in the center of the channel, as well as large westward events which encompass almost the entire channel (Fig. 12a). The along-channel pressure gradient term, follows closely the fluctuations of the across-channel current, but with smaller magnitude. The correlation is high across most of the channel, with the exception of the western side where the Yucatán current meanders. The advective term $\partial vu/\partial x$, which on average plays no role in the balance, shows considerable fluctuation on the Yucatán side with a negative correlation of -0.7 there and a correlation of 0.9 in the center of the channel (Figs. 13a and 13b), but remains without a significant contribution to the integrated along-channel balance. The remaining advective terms are negligible in the budget either at specific locations in the section or integrated across the channel. Hence, the balance remains practically geostrophic in the along-channel direction throughout the whole section.

EOF Analysis of altimetry and currents

In this section are compared the horizontal patterns of variability from altimetry with the vertical patterns of variability from the current. The spatial and temporal modes of variability were calculated from maps of SLA corresponding to the Yucatán Channel region, projected on an area of 1.5°X 2.1° with a 48 point mesh. The first SLA mode represents 57 % of the variability, with a two-lobe horizontal spatial structure and a meridional change of sign in sea level (Fig. 14a). The second mode explains 22 % of the variability and its horizontal spatial structure consists of a channel-centered lobe (Fig. 15a). Similarly, EOFs of the along-channel velocity in the upper 90 m surface layer were calculated using the objectively interpolated currents. The first mode explains 56 % of the variability and its vertical spatial structure represents a three-pole with flow in one direction in the center of the channel and in opposite direction along the sides of
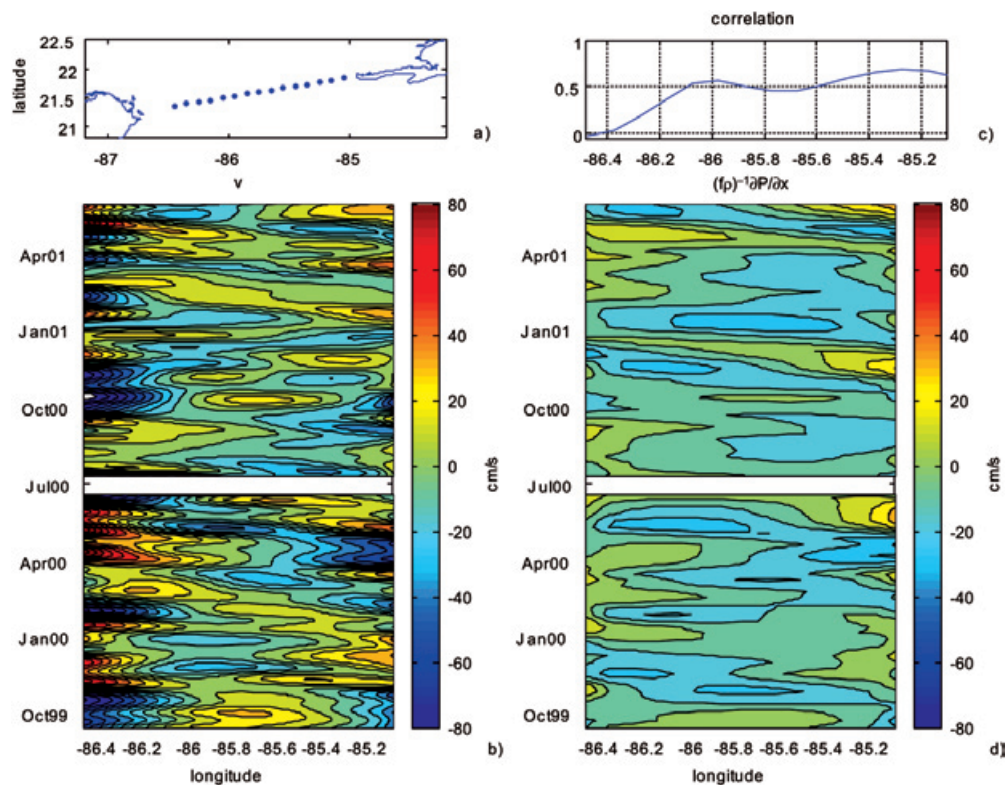
Fig. 10. a) Location of points where the across-channel momentum balance terms were calculated. b) Time series of the along-channel velocity. c) Correlation coefficient between the along-channel current and the across-channel pressure gradient as a function of cross channel position. d) across-channel pressure gradient.
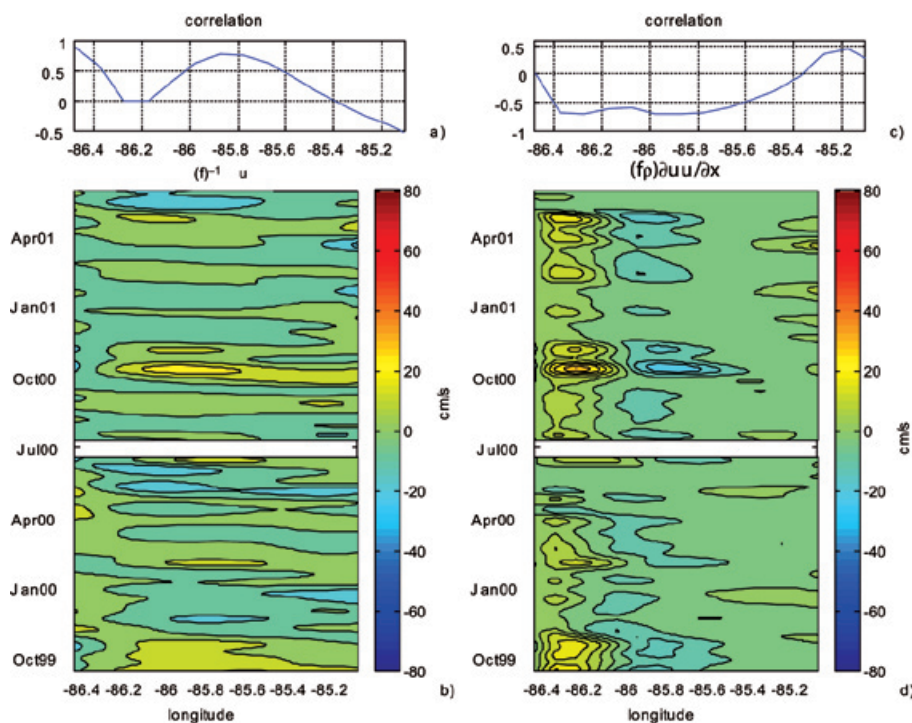

Fig. 11. a) Correlation coefficient between along-channel current and frictional term. b) Frictional term time series across the Yucatan channel. c) Correlation coefficient between velocity and $\partial uu/\partial x$ advective term. d) $\partial uu/\partial x$ advective term time series across the Yucatan channel.
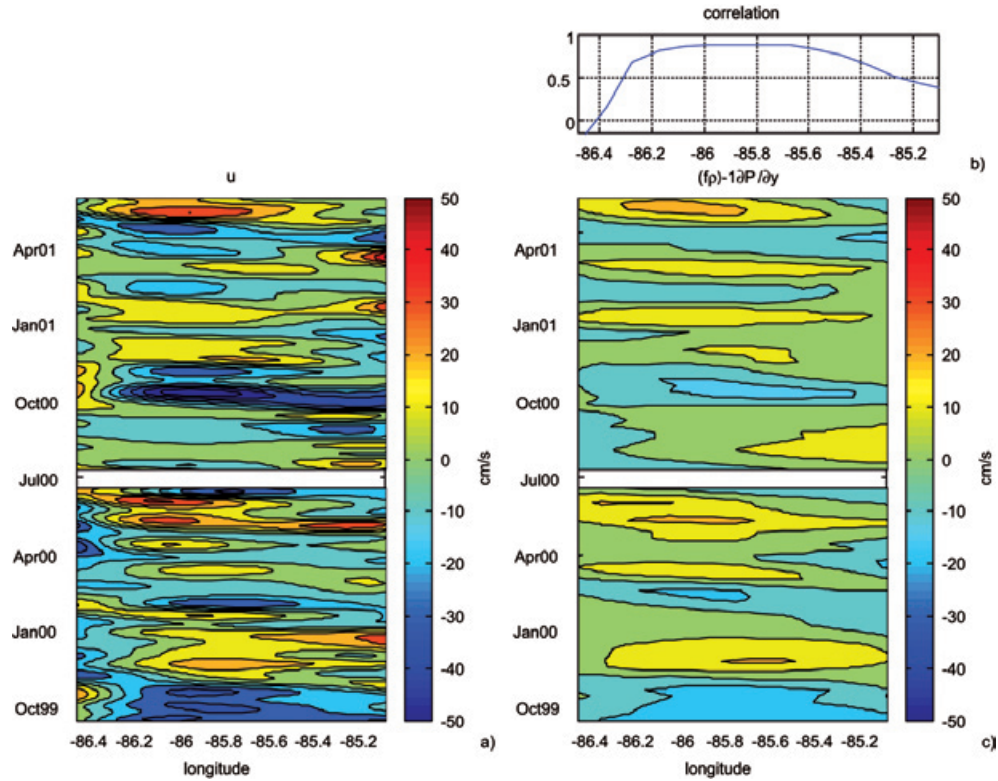
Fig. 12. a) Across-channel velocity time series across the Yucatan channel. b) Correlation coefficient between across-channel current and the along-channel pressure gradient as a function of cross channel position. c) Along-channel pressure gradient time series across the Yucatan channel.
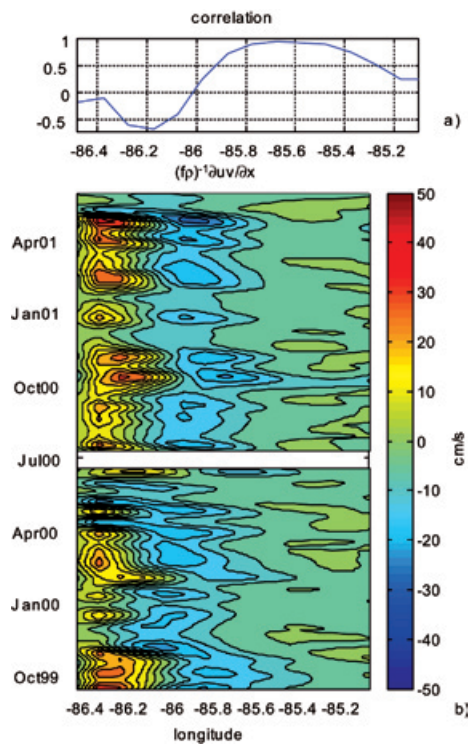

Fig. 13. a) Correlation coefficient between the across-channel current and $\partial vu/\partial x$ advective term. b) $\partial vu/\partial x$ advective term time series across the Yucatan channel.

the channel (Fig. 14b). The second mode represent 28 % of the variability and presents a vertical spatial two-pole structure where half of the channel has flow in one direction and the other half in the opposite direction (Fig. 15b). These results agree with the Yucatán Channel modes of variability calculated by Abascal et al. (2003) for the entire vertical cross-channel section as expected. The first modes for both SLA and flow might be interpreted like a passage of an anticyclone-cyclone pair through the channel, whereas the second modes of SLA and flow may correspond to the passage of an eddy through the center of the channel (Abascal et al., 2003; Candela et al., 2003).

EOFs of the sea level height are well related with the flow EOFs. The SLA EOF1 spatial structure represents a surface velocity pattern with marked shear oriented in the across-channel direction that is related with the flow EOF1 spatial structure. Also the surface velocity pattern associated to the SLA EOF2 spatial structure who shows strong sheared flow in along-channel direction is related with the flow EOF2 spatial structure. The principal components of modes 1 show a correlation coefficient of 0.59 for EOFs1 (Fig. 14c), but, the principal components of the second modes (horizontal for SLA, vertical for currents) are poorly correlated (Fig. 15c). Still, the spatial structures of both modes provide a strong suggestion that the flow variability in the upper 90 m surface layer of the
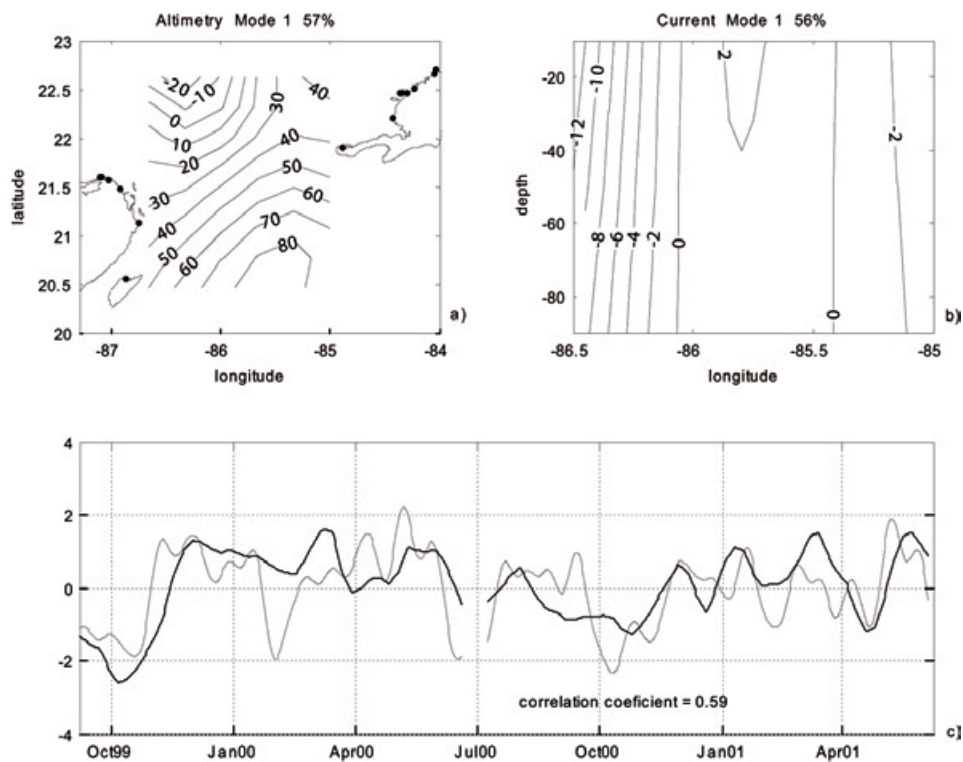
Fig. 14. a) First altimetry EOF mode spatial structure. b) First EOF mode spatial structure of the upper 90m surface layer current. c) Lower panel comparison between the principal components of the altimetry (bold line) and current (thin line) first EOFs.
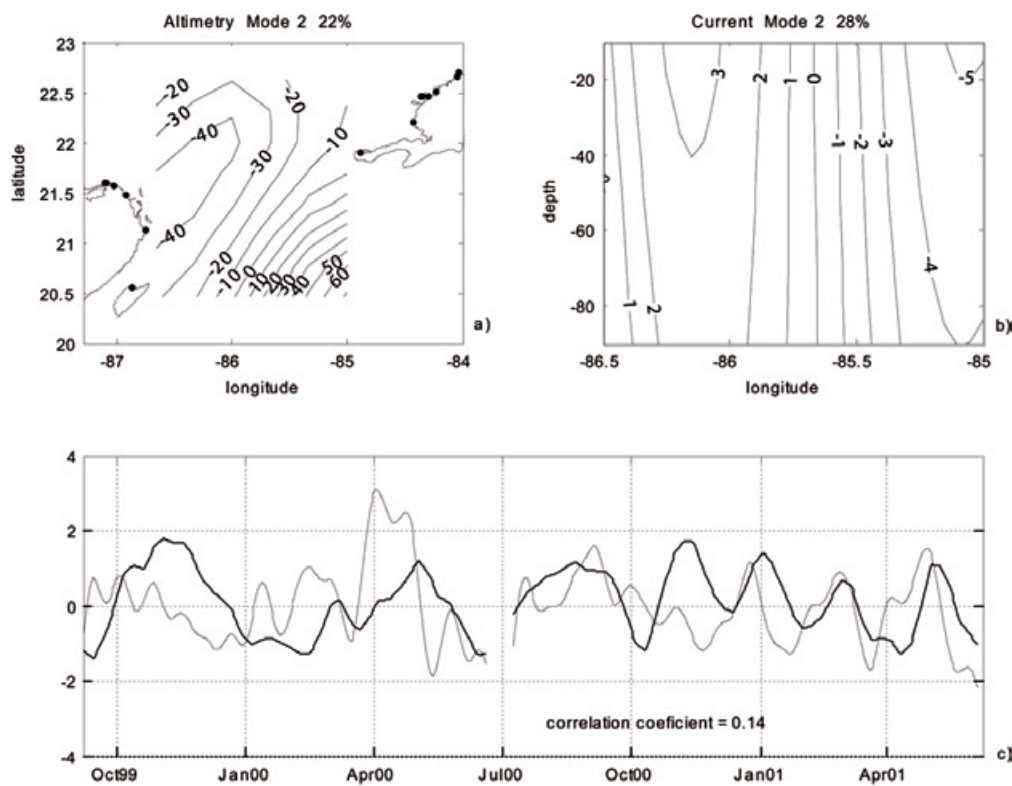

Fig. 15. a) Second altimetry EOF mode spatial structure. b) Second current EOF mode spatial structure of the upper 90m surface layer current. c) Comparison between the principal components of the altimetry (bold line) and current (thin line) EOFs.
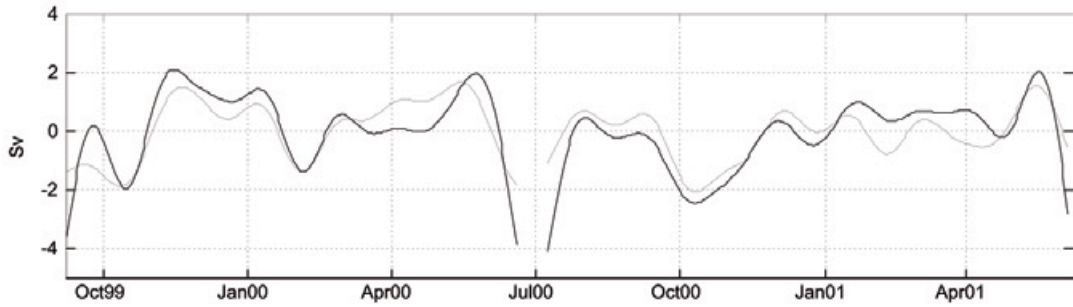
Fig. 16. Time series of the upper 90 m surface layer transport in the Yucatan channel (bold line) and the reconstructed transport time series with EOF1 of the along-channel current (thin line).

channel is related to that of the sea level. This relation between the sea surface dynamics and the flow through the channel was also found by Candela et al. (2003) in numerical simulations. In that study, a relationship was found between the surface current horizontal structure EOF with the vertical structure EOF of the flow, and the same surface spatial two-pole structure in EOF1 and surface centered pole in EOF2 were noted. Fig. 16 shows the transport time series in the upper 90 m surface layer of the channel and the reconstructed transport time series from EOF1, suggesting that EOF1 can extract almost the complete original transport time series, whence EOF1 represents the transport fluctuations in the channel and also seems to be associated with the SLA EOF1.

In order to better understand the transport fluctuations the ratio defined as $\{v'\}^2 / \{v'^2\}$ was calculated, where v' are the along-channel velocity anomalies, and the brackets denote a spatial average of the upper 90 m surface layer across the channel. Therefore $\{v'\}^2$ is the magnitude of the transport fluctuations and $\{v'^2\}$ is the kinetic energy density. This ratio is commonly used in analyzing the barotrophic versus baroclinic content of vertical profiles of velocity, where a ratio approaching 0 indicates a high cancellation of flow fluctuations in the vertical and a value of 1 indicates barotropic fluctuations (e.g. where there is no compensation and the flow is homogeneous in the vertical). However, the brackets imply an integration across the channel and over the upper 90 m surface
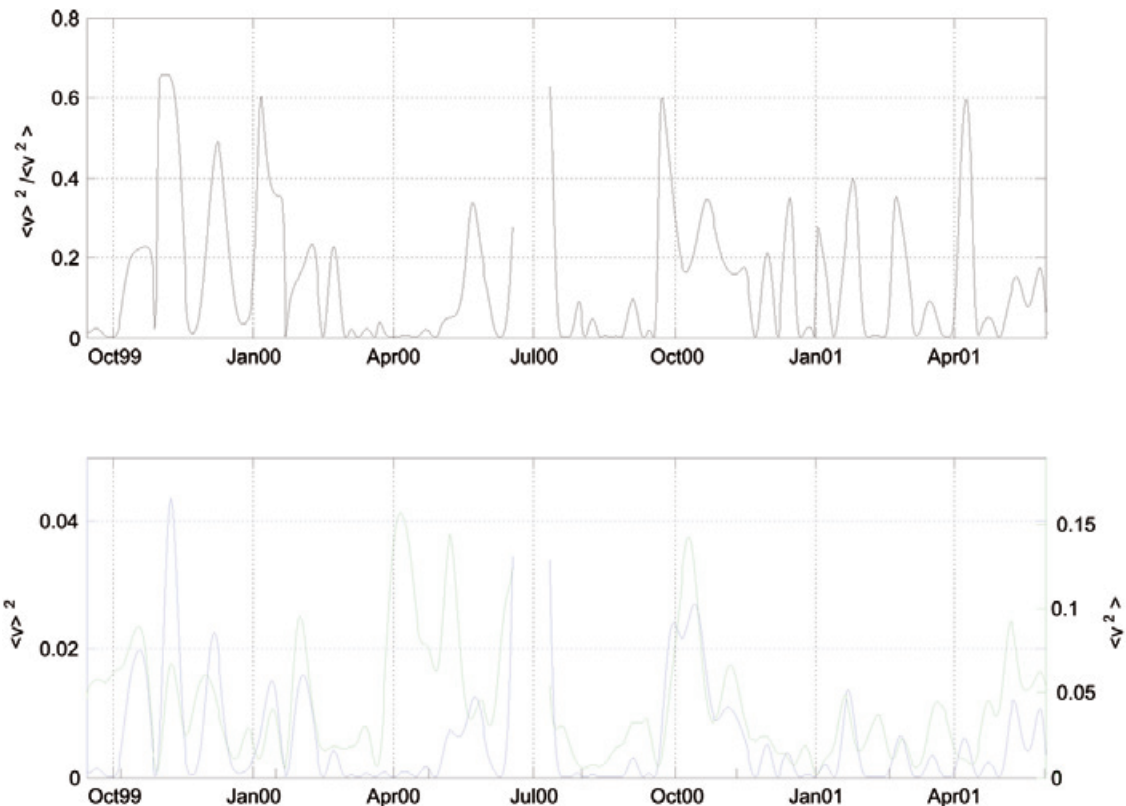

Fig. 17. Transport index in the upper 90 m surface layer (upper panel). Time series of $<v'>^2$ (blue, left-hand axis) and of $<v'^2>$ (green, right-hand axis).

layer, so index values of 1 or 0 do not necessarily imply barotropic or baroclinic motions. Abascal et al. (2003) found the ratio to be close to zero for the entire section of the Yucatán Channel, with an average value of 0.02 and maximum of 0.2, indicating that the fluctuations do not contribute significantly to the transport. We found for the upper 90 m surface layer that this ratio increases to an average of 0.15 and a maximum of 0.67 (Fig. 17), where most of the maximum events agree with extrema in the transport fluctuations. This suggests that in the surface layer of Yucatán Channel transport fluctuations are also related to energetic across-channel velocity fluctuations, which differs from the cancellation effect found by Abascal et al. (2003) for the entire section. Hence, if only the near surface layer of the channel is considered, where most of the transport and the largest current variability are found, the velocity fluctuations in fact to transport variations.

In order to better visualize the relation of the sea surface with the uppermost flow in the Yucatán Channel, the altimetry time series was interpolated to a transect across the channel, from which a geostrophic surface velocity was calculated according to:

$$\hat{v} = \frac{g}{f} \frac{\partial \eta}{\partial x} \quad , \tag{10}$$

where $\hat{v}$ is the geostrophic surface velocity, f is the Coriolis parameter and η the SLA. The geostrophic surface velocity thus obtained was decomposed into EOFs resulting in a first mode with a three-pole structure contributing 47% of the variability and a second mode representing a two-pole with 41% of the variability (Figs. 18a and 19a). Then comparing the time evolution of the geostrophic current EOFs deduced from altimetry with those of the upper 90 m surface layer currents across the channel, correlation coefficients of 0.29 for the first modes and of 0.74 for the second modes were obtained (Figs. 18c and 19c).

Discussion and summary

Geostrophic balance, which is commonly found in the across-channel direction in channels and straits also appears as the main balance in the along-channel direction in the Yucatán Channel. In the across-channel balance the frictional and Ekman drift terms also contribute importantly to the balance, especially during winter. This introduces the seasonal signal that is observed in the variability of along-channel velocity and pressure gradient terms, expressed as a correlation coefficient increase between the Ekman drift and pressure gradient terms with the along-channel velocity during winter.

The along-channel velocity as well as across-channel pressure gradient present spectral energy peaks at periods of 35 and 70 days. The 35 day peak seems to be related to the wind, whose Ekman flow also presents this energy peak, whereas the 70 day period peak, also present in the frictional term, could be related to current-eddy interactions. This speculation is supported by the terms in the along-channel balance, in which the across-channel velocity and the along-channel pressure gradient present coherent energy at the 70 day period band.

SLA in the channel and the flow in the upper 90 m are related as expressed by Candela et al. (2003) using surface velocities and the flow through the whole channel section from numerical simulations, with comparable mode structures. The time variability and spatial structures of the first modes are related to the upper-layer transport variability in the channel and present energy peaks at 125 and 200 days, while the second modes have peaks at 70 and 125 days. These periods of variability are the ones found in the across and along-channel balance terms (velocity, pressure gradient), and considering the results of Guerrero (2005) and Zhang et al. (2001), seem related to eddy-current interactions in the channel, which could also be affecting the observed transport variations.

An important relation exists between the geostrophic terms across-channel and along-channel but also the along-channel pressure gradient is associated with the transport fluctuations and these are tied to the Yucatán Current core movements. The meandering behavior of the Yucatán Current core has been attributed to the passage of eddy trains through the channel associated with variability of the current contained in EOF1 (Abascal et al., 2003). The upper 90 m surface layer of the channel shows that the core movement not only seems to be related to the EOF1 but also with the transport fluctuations and the along-channel pressure gradient. This meandering behavior of the current and transport fluctuations are similar to these in the Kuroshio Current, where the current meanders onshore (offshore) when the transport is high (low). Similarly in Yucatán, high transports correspond to an along-channel positive pressure gradient associated to a westward flow that moves the Yucatán Current core onshore. This is also manifested in the structure of the flow EOF1 having large positive currents at the sides of the channel. During a decrease in the transport there is a negative along-channel pressure gradient, and the velocity component u flows eastward and the Yucatán current core moves offshore, coinciding with the flow EOF1 structure having negative currents on both sides of the channel. Also the ratio $\{v'\}^2 / \{v'^2\}$ indicates that near surface transport fluctuations are related to energetic velocity fluctuations. Our results suggest that these energetic velocity fluctuations are related to the passage of eddies through the channel. Further studies are required to endorse this hypothesis.
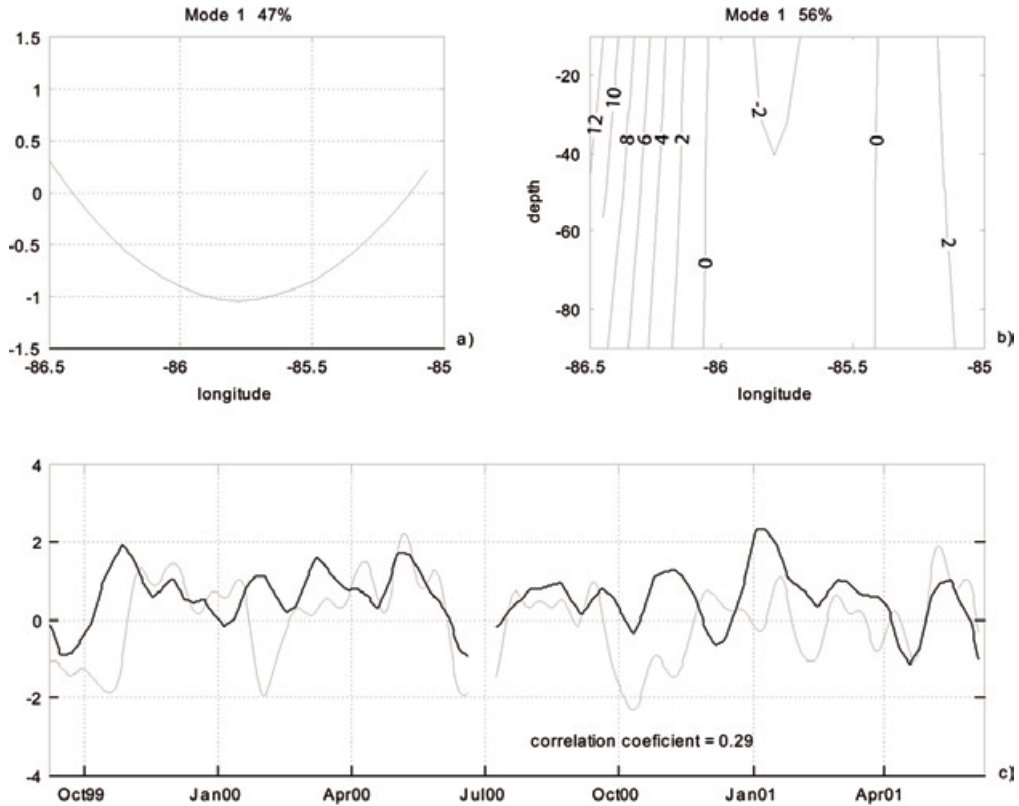
Fig. 18. a) EOF1 of geostrophic velocity from altimetry. b) current EOF1. c) Comparison between the principal components of the geostrophic velocity (bold line) and current (thin line) EOF1 modes.
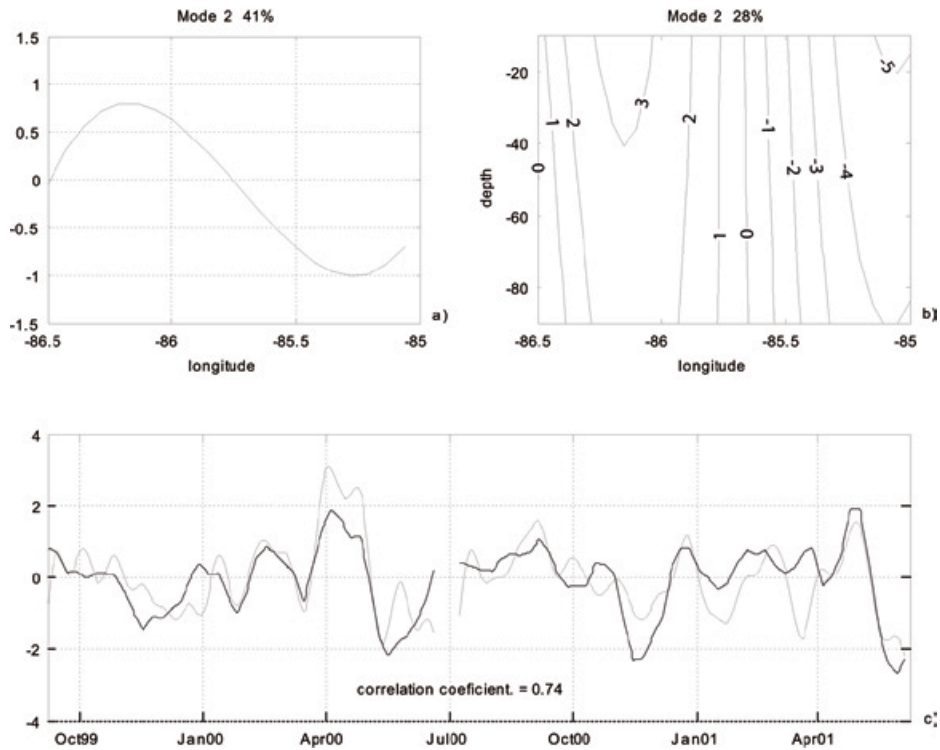

Fig. 19. a) EOF2 of geostrophic velocity from altimetry. b) current EOF2. c) Comparison between the principal components of the geostrophic velocity (bold line) and current (thin line) EOF2 modes.

Bibliography

Abascal, A., J. Sheinbaum, J. Candela, J. Ochoa and A. Badan, 2003. Analysis of flow variability in the Yucatán Channel, *Journal of Geophysical Research, 108 (C12)*, 3381, doi:10.1029/2003JC001922.

Anderson D. L. T. and R. A. Corry, 1985. Seasonal transport variations in the Florida Straits: a model study, *Journal of Physical Oceanography, 15*: 773-786.

Bryden H. L., 1997. Geostrophic comparisons from moored measurements of current and temperature during the Mid-Ocean Dynamics Experiment, *Deep-Sea Research, 44*: 667-681.

Bunge, L., J. Ochoa, A. Badan, J. Candela and J. Sheinbaum, 2002. Deep flows in the Yucatán Channel and their relation to changes in the Loop Current extension, *Journal of Geophysical Research, 107 (C12)*, 3233, doi:10.1029/2001JC001256.

Candela, J., C. Winant and H.L. Bryden, 1989. Meteorologically forced subinertial flows through the Strait of Gibraltar, *Journal of Geophysical Research, 94*: 12667-12679.

Candela, J., J. Sheinbaum, J. Ochoa and A. Badan, 2002. The potential vorticity flux through the Yucatán Channel and the Loop Current in the Gulf of Mexico, *Geophysical Research Letters, 29 (22)*,2059, doi:10.1029/ 2002GL015587,2002.

Candela, J., S. Tanahara, M. Crepon, B. Barnier and J. Sheinbaum, 2003. Yucatán Channel flow: Observations versus CLIPPER ATL6 and MERCATOR PAM models, *Journal of Geophysical Research, 108 (C12)*,3385,doi:10.1029/2003JC001961.

Cetina, P., J. Candela, J. Sheinbaum, J. Ochoa and A. Badan, 2006. Circulation along the Mexican Caribbean coast. *Journal of Geophysical Research, 111*, C08021 doi:10.1029/2005JC003056.

Chavez G., J. Candela and J. Ochoa, 2003. Subinertial flows and transports in Cozumel Channel, *Journal of*

Geophysical Research, 108 (C2), 3037, doi:10.1029/ 2002JC001456.

Emilsson I., 1971. Note on countercurrent in the Yucatán Channel and the western Cayman Sea, *Geofísica Internacional, 11*: 139-149.

Garret C. and B. Toulany, 1981. Variability of the flow through the Strait of Belle Isle, *Journal of Marine Research, 39*:163-189.

Johns W. E., T. N. Lee, D. Zhang and R. Zantopp, 2001. The Kuroshio East of Taiwan: moored transport observations from the WOCE PCM-1 array. *Journal of Physical Oceanography, 31*: 1031-1053.

Lee, T. N., F. Schott and R. Zantopp, 1985. Florida Current: Low-frequency variability of the Florida Current as observed with moored current meter stations during April 1982-June 1983 , Science, 227: 298-301.

Lee, T. N. and E. Williams, 1988. Wind-forced transport fluctuations of the Florida Current , *Journal of Physical Oceanography, 18*: 937-946.

Maul, G. A., D. A. Mayer and M. Bushnell, 1990. Statistical relationships between local sea level and weather with Florida-Bahamas cable and Pegasus measurements of Florida Current volume transport, *Journal of Geophysical Research, 95*: 3287-3296.

Murphy, S. J. and H. E. Hurlburt, 1999. The connectivity of eddy variability in the Caribbean Sea, the Gulf of México, and the Atlantic Ocean, *Journal of Geophysical Research. 104*:1431-1453.

Oey, L.-Y., 2004. Vorticity flux through the Yucatán Channel and Loop Current variability in the Gulf of Mexico, *Journal of Geophysical Research, 109*, C10004, doi:10.1029/2004JC002400,

Ochoa, J., J. Sheinbaum, A. Badan, J. Candela and D. Wilson, 2001. Geostrophy via potential vorticity inversion in the Yucatán Channel, *Journal of Marine Research. 59*: 725-747.

Ochoa, J., A. Badan, J. Sheinbaum and J. Candela, 2003. CANEK: measuring transport in the Yucatán Channel. Non-Linear Processes in Geophysical Fluid Dynamics. A tribute to the scientific work of Pedro Ripa. Ed. by O.U. Velasco Fuentes, J. Sheinbaum and J. Ochoa. Chap. 16, 275-286, Kluwer.

Ochoa, J., J. Candela, A. Badan and J. Sheinbaum, 2005. Ageostrophic fluctuactions in Cozumel Chan-

nel. *Journal of Geophysical Research, 110*, C02004, doi:10.1029/2004JC002408.

Percival D. B. and A.T. Walden, 1993. Spectral Analysis for Physical Applications, II edition, Cambridge University Press.

Pond, S. and G. L. Pickard, 1983. Introductory Dynamical Oceanography, 329 pp., Butterworth-Heinemann, Woburn, Mass.

Prandle D. and R. Player, 1993. Residual currents through the Dover Strait measured by H.F. radar, Estuarine, *Coastal & Shelf Science, 37*: 635-653.

Schmitz, W. J. Jr. and M. S. Mccartney, 1993. On the North Atlantic circulation, Reviews of Geophysics, 31,29-49.

Sheinbaum, J., J. Candela, A. Badan and J. Ochoa, 2002. Flow structure and transports in the Yucatán Channel, *Geophysical Research Letters, 29 (3)*, doi:10.1029/2001GL013990.

Tsimplis, M.N., 1997. Tides and sea-level variability at the Strait of Eripus, Estuarine, *Coastal & Shelf Science, 44*: 91-101.

Viúdez A., R. L. Haney and J. T. Allen, 1999. A study of the balance of horizontal momentum in a vertical shearing current, *Journal of Physical Oceanography, 30*: 572-589.

Zavala-Hidalgo J., S. L. Morey, J. J. O'Brien and L. Zamudio, 2006. On the Loop Current eddy shedding variability, *Atmósfera, 19 (1)*, 41-48,

Zhang D., N. T. Lee and W. E. Johns, 2001. The Kuroshio East of Taiwan: modes of variability and relationship to interior ocean mesoscale eddies, *Journal of Physical Oceanography, 31*: 1054-1074

M. Marín[1*], J. Candela[1], J. Sheinbaum[1], J. Ochoa[1] and A. Badan[1]
[1]Departamento de Oceanografía Física, Centro de Investigación Científica y Educación Superior de Ensenada, Ensenada, Baja California, México.
*Corresponding author: mmarin@cicese.mx